J Electroceram (2009) 23:376–381
DOI 10.1007/s10832-008-9471-9

Electrochemical characteristics of phosphorus doped silicon and graphite composite for the anode materials of lithium secondary batteries

Myung-ho Kong · Jae-hyun Noh · Dong-jin Byun · Joong-kee Lee

Received: 21 May 2007 / Accepted: 18 March 2008 / Published online: 13 April 2008

Abstract Poly-crystalline silicon particles with a diameter of 80~100 nm were synthesized by the plasma arc discharge method. Natural graphite, poly-crystalline silicon, poly-crystalline silicon/graphite composite and phosphorus doped poly-crystalline silicon/graphite composite particles were used as the anode materials of lithium secondary batteries and their electrochemical performances were compared. The phosphorus component on the surface and internal structure of the silicon particles were observed by XPS and SIMS analyses, respectively. In our experiments, the phosphorus doped silicon/graphite composite electrode exhibited better cycle performance than the intrinsic silicon/graphite composite electrode. The discharge capacity retention efficiency of the intrinsic silicon/graphite composite and phosphorus doped silicon/graphite composite electrodes after 20 cycles were 8.5% and 75%, respectively. The doping of phosphorus leads to an increase in the electrical conductivity of silicon, which plays an important role in enhancing the cycle performance. The incorporation of silicon into graphite has a synergetic effect on the mitigation of the volume change and conducting medium in the composite electrode during the charge–discharge reaction.

Keywords Lithium secondary battery · Phosphorus doping · Silicon · Anode · Composite

M.-h. Kong · J.-h. Noh · J.-k. Lee (✉)
Second Battery Research Center,
Korea Institute of Science and Technology,
P.O. Box 131, Cheongryang, Seoul 130-650, South Korea
e-mail: leejk@kist.re.kr

M.-h. Kong · D.-j. Byun
Department of Material Science & Engineering, Korea University,
Seoul 136-713, South Korea

1 Introduction

Graphite, which has a theoretical capacity of 372 mA h/g, is used commercially as an anode material for lithium secondary batteries, due to its excellent cycle stability and low cost [1]. However, as an anode material in lithium secondary batteries, graphite has a significant shortcoming in that its initial capacity is low [2–3]. In order to increase the specific capacity of lithium secondary batteries, silicon with its high theoretical capacity (e.g., 4,000 mA h/g) has been employed as an alternative negative electrode material. The employment of silicon as an anode material, however, has difficulties for the following reasons: (a) the poor cycle performance due to the large volume changes that occur during repeated alloying/de-alloying reactions, and (b) the low electrical conductivity of silicon itself. The disadvantages of using silicon as the anode material for lithium secondary batteries are consequently related to its poor electrical conductivity and the drastic volume changes that occur during the charging–discharging process [4–6].

In order to solve these problems, composite electrodes materials, in which silicon particles are mixed with conducting materials such as metals and oxides, have been investigated. For instance, Mg_2Si exhibits a high initial capacity, but its cycle life is too short to use in commercial applications. The rapid failure of the electrode was attributed to the large volume changes associated with the formation of Li–Mg and Li–Si during the repeated alloying/de-alloying reactions during cycling. These alloys result from the decomposition of the Li_xMg_2Si solid solution or ternary Li_2MgSi phase during lithiation. There is some controversy as to the actual reaction mechanism of Mg_2Si with lithium at ambient temperature [7]. Recently, Idota et al. [8] suggested that tin oxide composites could be used as an alternative to graphite for the anodes in lithium-ion cells.

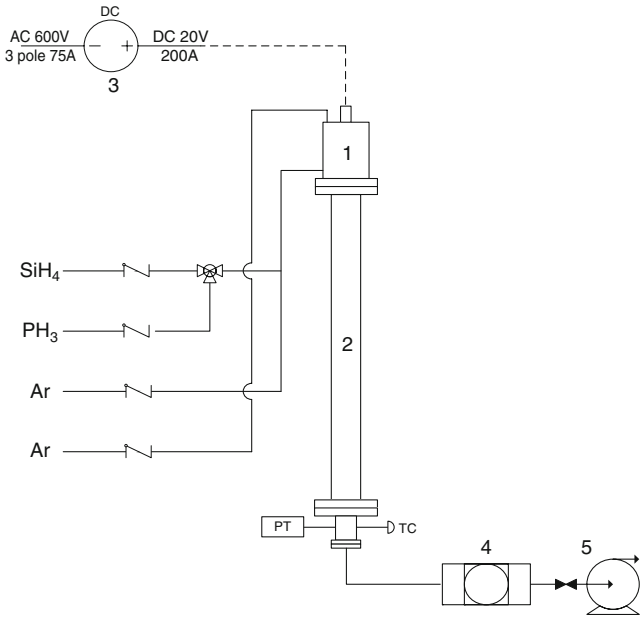

Fig. 1 Schematic diagram of plasma arc discharge method for synthesizing poly-crystalline silicon particles; (*1*) plasma torch, (*2*) reaction tube, (*3*) DC power supply, (*4*) filter, (*5*) vacuum pump

These new anodes are claimed to have theoretical volumetric and gravimetric capacities that are four and two times higher than those of carbon, respectively. The best results so far have been obtained with amorphous SnO doped with various elements such as B, Al and P. These promising findings have attracted the attention of several research groups investigating the ability of SnO_2, an n-type semiconductor commonly used in conductivimetric sensors, to act as an insertion electrode in lithium cells [9]. The purpose of this work is to investigate the effect of phosphorus doping into silicon particles on the electrochemical performance of the anode material of lithium secondary batteries. We expected that the higher conductivity of silicon afforded by phosphorus doping would improve the cycle performance.

2 Experimental

2.1 Preparation

Four different kinds of anode materials for lithium secondary batteries were prepared in this study; (a) spherical shaped natural graphite with a diameter of 20 μm (S0), (b) intrinsic silicon particles synthesized by the decomposition of SiH_4 under arc plasma (S1) (c) synthesized intrinsic silicon/graphite composite (S2), and (d) synthesized phosphorus doped silicon/graphite composite (S3). The phosphorus doped silicon particles were prepared by the decomposition of SiH_4 and PH_3 under arc plasma.

Table 1 Experimental conditions for preparation of poly-crystalline silicon particles.

Process parameter	Intrinsic silicon	Phosphorus doped silicon
DC power (kW)	4	4
Ar flow rate (l min^{-1})	12	12
SiH_4 flow rate (sccm)	45	45
PH_3 flow rate (sccm)	N.A.	9
Reaction time (min)	30	30

2.2 Synthesis of silicon particles

Poly-crystalline silicon particles were prepared by the plasma arc discharge method. A schematic diagram of the arc plasma system is shown in Fig. 1. It consists of a (1) plasma torch, (2) reactor, (3) DC power supply, (4) filter and (5) vacuum pump. The plasma torch consists of a tungsten anode and copper cathode. The reactor is made of an annular type tube for cooling purposes. The plasma generating power is kept constant at 4 kW with 20 V/200 A, and argon flow into the plasma torch is used to generate the plasma arc flame. For the preparation of the intrinsic silicon particles, silane (SiH_4) gas is fed into the upstream of the plasma torch which is placed in the top of the reactor. For the preparation of the phosphorus doped silicon, PH_3 gas mixed with SiH_4 gas is injected into the reactor. The detailed experimental conditions are shown in Table 1. The synthesized particles were collected by a

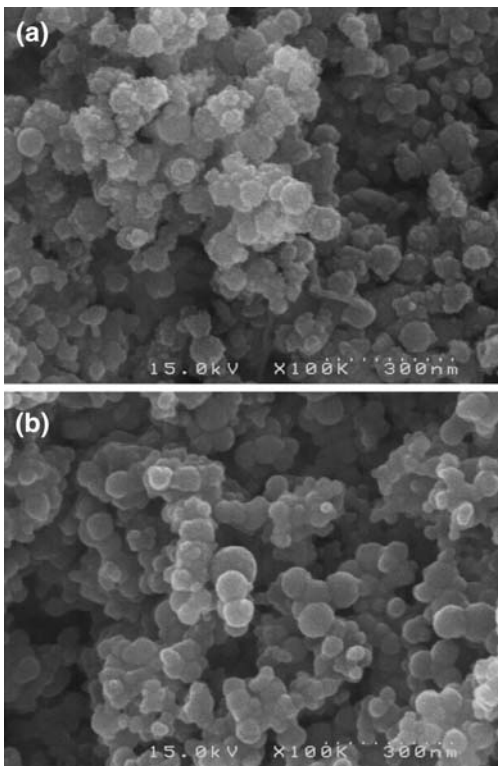

Fig. 2 Scanning electron microscopy images of synthesized silicon particles; (**a**) intrinsic silicon particles, (**b**) phosphorus doped silicon particles

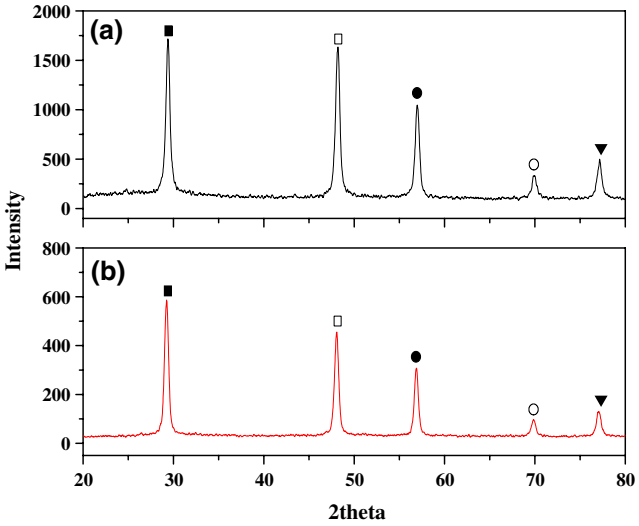

Fig. 3 X-ray diffraction patterns of synthesized silicon particles; (**a**) intrinsic silicon particles, (**b**) phosphorus doped silicon particles; *filled square* (111), *empty square* (220), *filled circle* (311), *empty circle* (400), *inverted filled triangle* (331)

Teflon filter which is placed inside the particle collector and these particles are used as the working electrode material of a lithium half cell.

2.3 Manufacture of silicon/graphite composites

In order to manufacture the silicon/graphite composite, we mixed synthesized silicon and natural graphite with mortar and then dispersed them by ultrasonication for 10 min in methanol. After their complete dispersion, we dried the mixture at 60°C for 24 h in a vacuum oven. The drying process is necessary to evaporate the moisture in the particles with methanol. After drying, we crushed the conglomerated mixture and sieved the particles with a mesh (75 μm).

2.4 Analyses

The doping aspect of the synthesized samples was characterized by X-ray diffraction (XRD, Rigaku Miniflex) with CuKα radiation and secondary ion mass spectrometry (SIMS, PHI 7200). X-ray photoelectron spectroscopy (XPS, VG Scientific ESCALAB 200R) was used to verify the transition of the binding energy in the Si2p or P2p3 peak. The X-ray source was MgKα (1486.6eV) and a concentric hemispherical analyzer was used. The surface microstructures of the synthesized particles were investigated by scanning electron microscopy (SEM). In order to measure the electrical bulk resistivity, AC (alternative current) measurements were performed on the intrinsic silicon/graphite composite, phosphorous doped silicon/graphite composite and natural graphite in the frequency range from 0.01 to 10^5 Hz (ZAHNER IM6). The intrinsic silicon was excluded from these measurements, because its resistivity is too high to measure.

2.5 Cell fabrication and electrochemical evaluation

Half cells were fabricated with Li metal foil as a counter electrode to compare the electrochemical performances of the various anode materials [10]. The natural graphite, intrinsic silicon, intrinsic and phosphorus doped silicon/graphite composites electrodes containing 10 wt.% poly vinylidene fluoride (PVDF) binder, acetylene black (AB) 10 wt.% conductor were prepared by a casting method in a dry room (max. moisture <0.5%). The electrolyte employed in this study was 1M $LiPF_6$ dissolved in a 1:1:1 (volume/volume) mixture of ethylene carbonate (EC), ethyl–methyl carbonate (EMC) and dimethyl carbonate (DMC), and polypropylene film was adopted as a separator. All of the cells were galvanostatically charged and discharged in the voltage range from 0 to 2 V versus Li/Li^+ under a current density of 30 mA h/g (Maccor SERIES 4000).

3 Results and discussion

The SEM was employed to investigate the characteristics of the surface morphologies for the synthesized intrinsic and phosphorus doped silicon particles. Figure 2 shows the surface morphology of the intrinsic and phosphorus doped silicon particles which show that the agglomerates consist of spherical particles with a diameter of 80~100 nm. Comparing Fig. 2(a) and (b), the particle diameter for the

Table 2 X-ray diffraction peaks' parameters and crystalline sizes.

Intrinsic silicon					Phosphorus doped silicon				
2θ	d (Å)	FWHM(B)	I/Io	L_c (Å)	2θ	d (Å)	FWHM(B)	I/Io	L_c (Å)
29.40	3.03539	0.447	100	191.905	29.28	3.04756	0.588	100	145.847
48.20	1.88635	0.494	96	184.002	48.14	1.88856	0.565	74	160.842
56.98	1.61477	0.471	62	200.438	57.02	1.61373	0.541	50	174.536
69.86	1.34525	0.471	20	214.874	70.04	1.34223	0.235	17	431.136
77.18	1.23489	0.306	29	346.911	77.18	1.23489	0.729	21	145.617

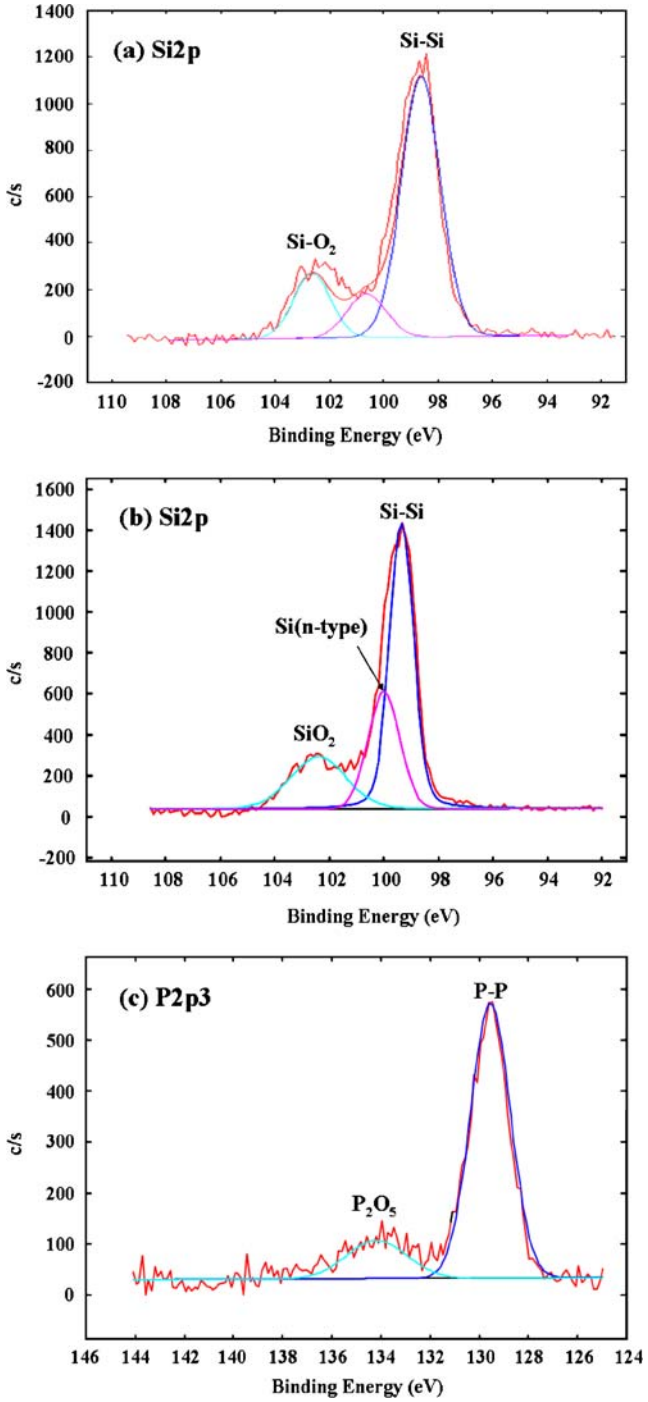

Fig. 4 X-ray photoelectron spectroscopy for Si2p and P2p3 spectra; (**a**) intrinsic silicon particles at Si2p, (**b**) phosphorus doped silicon particles at Si2p, (**c**) phosphorus doped silicon particles at P2p3

intrinsic and phosphorus doped silicon particles is almost the same, but the intrinsic silicon particles seem to have a rougher surface.

The XRD patterns for the synthesized intrinsic and phosphorus doped silicon particles are shown in Fig. 3. As shown in this figure, they have a poly-crystalline structure with (111), (220), (311), (400), and (331) diffractions. No diffraction peaks corresponding to free phosphorus or its compounds were observed in the spectra. Comparing the diffraction pattern between the two materials, the phosphorus doped silicon has lower peak intensity than the intrinsic silicon. This difference in intensity is caused by phenomena such as the crystallographic structure, the position of the atoms within the elementary cell and their thermal vibrations. There was no difference in the crystallographic structure of the two materials, because the 2-theta angle of the two patterns is almost the same for both samples. This means that the lower peak intensity of the phosphorus doped silicon is due to the change in the thermal vibration caused by the addition of phosphorus atoms. In fact, we found that the crystal size is obviously decreased at 2-theta values of around 29°, 48°, 57° and 77°, which correspond to the (111), (220), (311) and (331) lattice planes, respectively. The crystal sizes were calculated by the Debye–Scherrer equation as follows [11].

$$B = 0.9\lambda / L_c \cdot \mathrm{Cos}\theta \quad (1)$$

where B is the full width of half maximum [Å], λ is the wavelength of the CuKα radiation [Å], and L_c is the crystal size [Å].

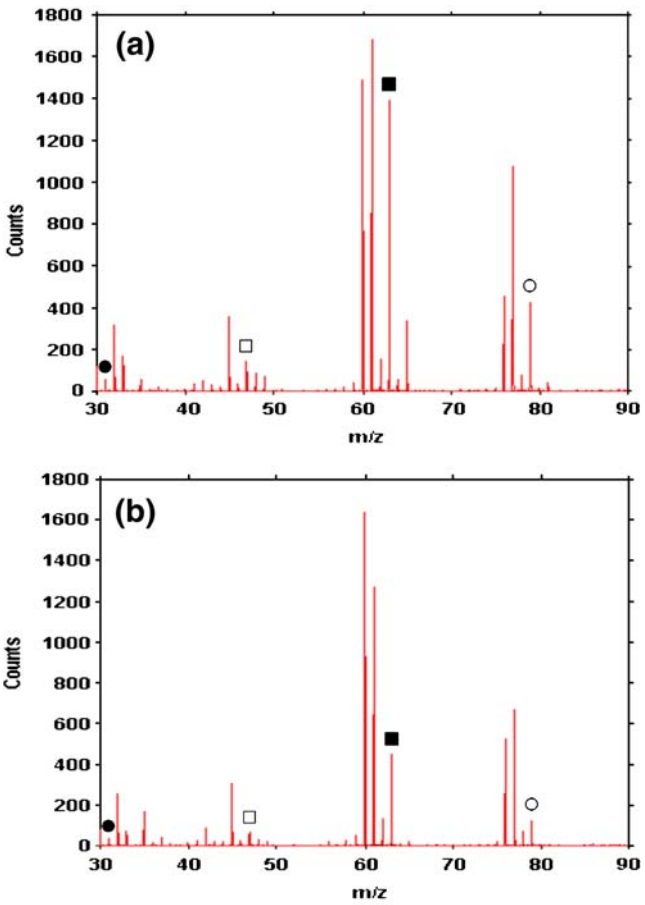

Fig. 5 Secondary ion mass spectrum of phosphorus doped silicon particles; (**a**) at surface, (**b**) after cleaning; *filled circle*: P, *empty square*: PO, *filled square*: PO_2, *empty circle*: PO_3

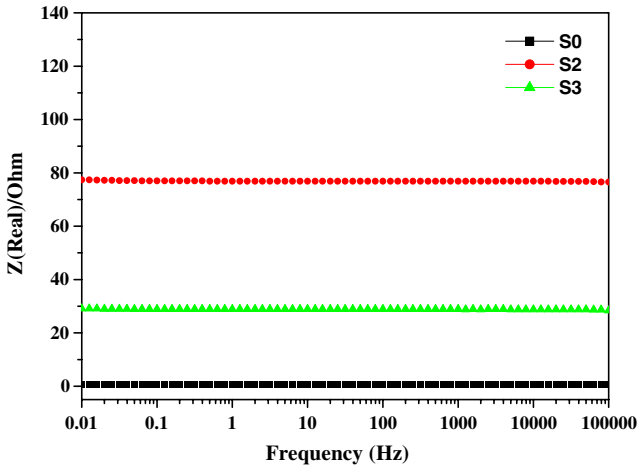

Fig. 6 AC current plot for bulk resistivity of S0, S2, S3 in range of 0.01~10^5 Hz, ac amplitude 5 mV (*S0*: natural graphite, *S2*: intrinsic silicon/graphite composite, and *S3*: phosphorus doped silicon/graphite composite)

The calculated crystal sizes are shown in Table 2. The above results indicate that the synthesize of phosphorus doped silicon particles by the plasma arc discharge method produces poly-crystalline silicon with a face centred cubic (FCC) structure, in which some of the silicon atoms are substituted by phosphorus. It seems that the increase of the particle size at a 2-theta value of around 70° is caused by various forms of phosphorus oxide. X-ray photoelectron spectroscopy (XPS) and secondary ion mass spectroscopy (SIMS) analyses were employed to determine the amount of phosphorus oxides, because they were too small to be measured using XRD.

The XPS measurements were carried out for the intrinsic and phosphorus doped silicon particles to investigate the bonding of phosphorus within them. Figure 4 shows the Si2p and P2p3 spectra. All of the peaks were classified according to their binding energy. The Si2p spectrum for the intrinsic poly-crystalline silicon in Fig. 4(a) shows peaks for SiO_2 and Si–Si bonds at 102.5 and 98.6 eV, respectively [12]. However, the Si2p spectrum of the phosphorus doped poly-crystalline silicon in Fig. 4(b) shows peaks for SiO_2, Si–Si and n-type Si at 103.3, 99.5 and 100 eV, respectively, while the P2p3 spectra in Fig. 4(c) shows peaks for the P–P and P_2O_5 bonds at 129.5 and 134.9 eV, respectively [13]. The presence of phosphorus atoms in the silicon was confirmed by the n-type Si peak and the existence of P–P and P_2O_5 bonds.

The SIMS was carried out to study the extremely small quantity of phosphorus atoms in the P-doped silicon particles. A Cs^+ ion beam energy of 7.9 keV was used to investigate the negative ion SIMS spectra. We analyzed the phosphorus doped silicon particles in static mode and found small amounts of phosphorus and various forms of phosphorus oxide both on the surface of and inside the particles. Figure 5(a) shows the P, PO, PO_2, PO_3 peaks of the SIMS spectra at the surface and Fig. 5(b) shows the peaks of the phosphorus and phosphorus oxides remaining after cleaning. These results support the theory that the phosphorus oxides have an effect on the crystal size of the synthesized silicon particles at 2-theta values of around 70° in the XRD pattern.

The electrical bulk resistivity of the graphite and composite materials were measured by the AC method with a four-point-probe tool. Figure 6 shows that the natural graphite exhibits the lowest electrical bulk resistivity among the samples, while the intrinsic silicon/graphite composite exhibits the highest. In the case of the phosphorus doped silicon/graphite composite, the electrical bulk resistivity was lower than that of the intrinsic silicon composite.

Figure 7 shows the variation of the discharge capacity with the number of cycles. As shown in this figure, the capacity fading of S3 is lower than that of S2. The lower capacity fading of S3 is closely related to the electrical bulk resistivity of its composite material, as shown in Fig. 6. Even though the content of phosphorus in the silicon is very low, it plays an important role in enhancing the capacity retention. These results indicate that the smaller electrical bulk resistivity of the material affects the cycle performance of the electrode. As described above, a mixture of synthesized nano-sized silicon particles and natural graphite with a diameter of 20 μm is used for the composite materials. We believe that the enhancement of the specific capacity and cyclic performance of the composite is due to the synergetic effect of the excellent cycling behavior of graphite and the large specific capacity of the silicon material. Furthermore, the doping of

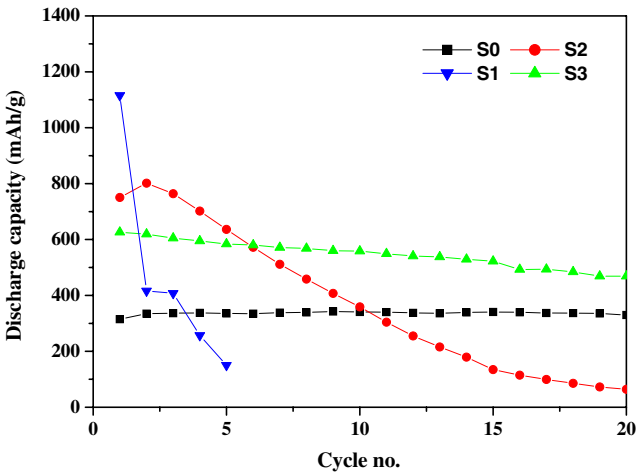

Fig. 7 Discharge capacity curves of *S0*, *S1*, *S2*, *S3* depend on cycle number; containing 1 M $LiPF_6$, EC + EMC + DMC (1:1:1 in *v*/*v*) electrolyte, cut-off voltage 0~2 V, current density 30 mA h/g (*S0*: natural graphite, *S1*: intrinsic silicon, *S2*: intrinsic silicon/graphite composite, and *S3*: phosphorus doped silicon/graphite composite)

phosphorus is found to be the key process for the improvement of the cycle retention through the enhancement of the conductivity of the composite [14]. However, in the case of the material containing silicon, the degradation of the cycle performance is still observed, due to the volume changes during cycling, even though the graphite phase mitigates the electrode cyclability by acting as a mechanical and electrochemical buffer in the composite [15]. The volume expansion of silicon during its alloying with lithium, leading to the formation of cracks which generate a dead volume, and the subsequent volume shrinkage during de-alloying, generate an electronically inactive zone which is isolated from the electron transport path [16, 17].

4 Conclusion

In this study, we propose that phosphorus doping into silicon provides an electron transport path for the isolated inactive material caused by the severe volume changes of the silicon electrode. The phosphorus doped silicon/graphite exhibited a lower bulk resistivity than the intrinsic silicon/graphite under the same experimental conditions. The characteristics of the synthesized silicon particles were investigated to determine their structure and the chemical bonding status of the phosphorus atoms using XRD, XPS, SEM and SIMS. The lower bulk resistivity of the phosphorus doped silicon/graphite was explained by the finding that the plasma arc discharge method does not alter the structure of the polycrystalline silicon in spite of the doping of phosphorus atoms. The phosphorus doped silicon/graphite composite shows better capacity retention than the intrinsic silicon/graphite composite after 20 cycles. It was also observed that graphite acted as a conducting medium which synergistically contributed to the cycle performance.

Acknowledgement This research was supported by a grant (code #05K1501-01920) from the 'Center for Nanostructured Materials Technology' under the '21st Century Frontier R&D Programs' of the Ministry of Science and Technology, Korea.

References

1. I.C. Kim, D. Byun, J.K. Lee, Journal of Electroceramics **17**, 661–665 (2006)
2. S. Flandrois, B. Simon, Carbon **37**, 165–180 (1999)
3. B. Simon, S. Flandrois, K. Guerin, A. Fevrier-Bouvier, I. Teulat, P. Biensan, J. Power Sources **81**, 312–316 (1999)
4. J.H. Ryu, J.W. Kim, Y.E. Sung, S.M. Oh, Electrochem. Solid-State Lett. **7**, A306–A309 (2004)
5. J.W. Kim, J.H. Ryu, K.T. Lee, S.M. Oh, J. Power Sources **147**, 227–233 (2005)
6. C. Wang, A.J. Appleby, Frank E. Little, J. Power Sources **93**, 174–185 (2001)
7. G.A. Nazri, *Lithium Batteries Science and Technology* (Kluwer, Boston, 2004), pp. 260–266
8. Y. Idota, T. Kubota, A. Matsufuji, Y. Maekawa, T. Miyasaka, Science **276**, 1395 (1997)
9. J. Morales, L. Sa'nchez, Solid State Ion. **126**, 219–226 (1999)
10. J.H. Lee, Y.M. Choi, U. Paik, J.G. Park, Journal of Electroceramics **17**, 657–660 (2006)
11. B.D. Cullity, *Elements of X-ray Diffraction, Chap 9*, 2nd edn. (Addison-Wesley, London, 1978), pp. 346–352
12. http://www.lasurface.com/database/liaisonxps
13. J.F. Moulder, W.F. Stikle, P.E. Sobol, K.D. Bomben, *Handbook of X-ray Photoelectron Spectroscopy* (Physical Electronics, Minnesota, 1995), p. 238 Appendix B. Chemical states Tables
14. S. Dimitrijev, *Principles of Semiconductor Devices* (Oxford University Press, New york, 2006), pp. 15–16
15. X.Q. Yang, J. McBreen, W.S. Yoon, M. Yoshio, H. Wang, K. Fukuda, T. Umeno, Electrochem. Commun. **4**(11), 893–897 (2002)
16. Z. Chen, L. Christensen, J.R. Dahn, Electrochem. Commun. **5**, 919–923 (2003)
17. L.Y. Beaulieu, T.D. Hatchard, A. Bonakdarpour, M.D. Fleischauer, J.R. Dahn, J. Electrochem. Soc. **150**(11), A1457–A1464 (2003)